OPEN

Sensitive Real-Time Monitoring of Refractive Indexes Using a Novel Graphene-Based Optical Sensor

Fei Xing[1], Zhi-Bo Liu[1], Zhi-Chao Deng[1], Xiang-Tian Kong[1], Xiao-Qing Yan[1,2], Xu-Dong Chen[1], Qing Ye[1], Chun-Ping Zhang[1], Yong-Sheng Chen[2] & Jian-Guo Tian[1]

[1]The Key Laboratory of Weak Light Nonlinear Photonics, Ministry of Education, Teda Applied Physics School and School of Physics, Nankai University, Tianjin 300071, China, [2]The Key Laboratory of Functional Polymer Materials and Center for Nanoscale Science & Technology, Institute of Polymer Chemistry, College of Chemistry, Nankai University, Tianjin 300071, China.

Correspondence and requests for materials should be addressed to Z.-B.L. (nkzbliu@gmail.com) or J.-G.T. (jjtian@nankai.edu.cn)

Based on the polarization-sensitive absorption of graphene under conditions of total internal reflection, a novel optical sensor combining graphene and a microfluidic structure was constructed to achieve the sensitive real-time monitoring of refractive indexes. The atomic thickness and strong broadband absorption of graphene cause it to exhibit very different reflectivity for transverse electric and transverse magnetic modes in the context of a total internal reflection structure, which is sensitive to the media in contact with the graphene. A graphene refractive index sensor can quickly and sensitively monitor changes in the local refractive index with a fast response time and broad dynamic range. These results indicate that graphene, used in a simple and efficient total internal reflection structure and combined with microfluidic techniques, is an ideal material for fabricating refractive index sensors and biosensor devices, which are in high demand.

In recent years, graphene has emerged as a novel two-dimensional (2D) material in the field of materials science due to its prominent intrinsic electronic, thermal, mechanical, structural and chemical properties[1]. Highly sensitive biosensors and electrochemical sensors based on graphene field-effect transistors have been widely developed for sensing gases[2,3], liquids[4,5] and biomolecules[6–8]. Because graphene has a 2D structure, with each of its atoms exposed, its electrical properties are very sensitive to changes in the charge environment induced by the reaction or adsorption of analytes on its surface. However, a transistor-based graphene sensor requires the measuring of current changes on the graphene surface; therefore, the temporal and spatial resolution is greatly restricted relative to that of optical sensors. Due to its high carrier mobility and zero-bandgap characteristics, graphene exhibits unique and desirable optical properties, such as broadband and tunable absorptions[9,10] and strong polarization-dependent effects[11–14]. Thus, new high-performance graphene-based optical sensors are expected to be capable of characterizing surface structural changes and biomolecular interactions.

For optical sensors, measurements of refractive index changes are important for a variety of applications in biosensing, drug discovery, environmental monitoring, and gas- and liquid-phase chemical sensing. Various methods for obtaining these measurements have been developed[15]. At present, refractive-index-sensing technologies based on surface plasmon resonance (SPR) are widely used based on their ability to provide highly sensitive label-free real-time data[16]. The most common modulation approaches used in high-performance SPR sensors are based on the spectroscopy of surface plasmons in wavelength or angular domains. However, when measuring a range of wavelengths or angles, optical focusing limits the sensitivity, resolution, dynamic range and other functionalities of a spectroscopy-based SPR instrument and produces notable deficiencies in the real-time performance (>ms) of the sensor in question. An SPR sensor with amplitude modulation can produce fast, real-time monitoring and imaging functions, but its performance is typically worse than that of spectroscopy-based SPR sensors. Moreover, biomolecules adsorb poorly on gold, limiting the sensitivity of conventional SPR biosensors.

In this study, we present a strategy for sensing changes in refractive indexes using graphene optical sensors; in particular, this strategy is based on the different reflection behaviors of transverse-magnetic (TM) and transverse-electric (TE) modes under total internal reflection conditions. The model used in this investigation consists of a graphene layer sandwiched between a high-index medium (medium 1, refractive index n_1) and a low-index medium (medium 2, refractive index n_2) (Fig. 1a). As has been observed for the SPR sensor, the differences in
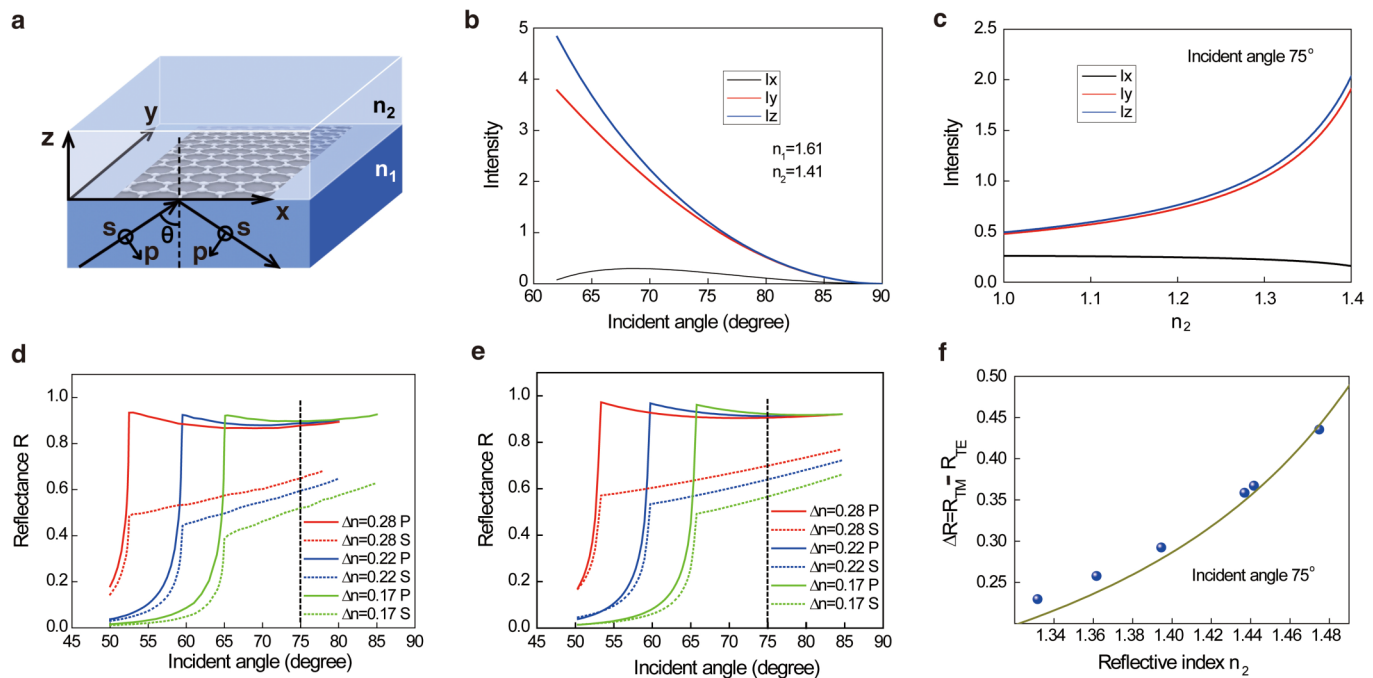
Figure 1 | The polarization-dependent features in graphene sandwiched structure. (a) A schematic illustration of graphene sandwiched between two dielectric layers. (b) A plot of the intensities of the evanescent waves for the x and z components at p-polarization and the y component at s-polarization with different incident angles. (c) A plot of the intensities of the evanescent waves for the x and z components at p-polarization and the y component at s-polarization with different refractive indexes n_2. The incident angle is 75°. (d) The experimental results of reflectance for s- and p-polarized light with different $\Delta n = n_1 - n_2$ using a derivative total reflection method. (e) The theoretical results of reflectance for s- and p-polarized light with different Δn based on Maxwell's boundary conditions. (f) The experimental (circles) and theoretical (line) results of ΔR with different refractive indexes n_2.

reflectance between the TE and TM modes are sensitive to variations in the refractive index n_2 under fixed n_1 conditions. Therefore, using a graphene sensing layer, a change of refractive index with broad dynamic range can be measured under total internal reflection. The polarization-dependent absorption effect of graphene allows us to use the balanced detection scheme. The balanced detection solves the problems of real-time detection, and improves the measurement sensitivity. With intensity modulation, the graphene-based refractive index sensor (GRIS) assessed in this study demonstrates a high sensitivity of 10^5 per refractive index units (RIU^{-1}), a fast real-time response of ~10 μs, and a large dynamic range with $\Delta n > 0.5$, where $\Delta n = n_1 - n_2$ is the difference in refractive indexes between medium 1 and medium 2. Because the detection limit depends only on the signal-to-noise ratio, the detector sensitivity and the response time of the detector, GRIS is expected to achieve high sensitivity and fast response time easily. Furthermore, the various advantages of graphene, such as its stability, low cost, rich functionality, easily controlled thickness, and strong mechanical strength, make it a promising candidate for refractive index sensing and indicate its potential for wider applications, particularly in biological and chemical sensing.

Results

Polarization-dependent reflection and absorption. Due to its unique electronic structure, in which conical-shaped conduction and valence bands meet at the Dirac point, a pristine monolayer of graphene that has been scaled to an atomic thickness demonstrates frequency-independent optical conductance and strong broadband absorption per unit mass ($\pi \alpha = 2.3\%$)[17]. Moreover, its unique polarization-dependent effects[11,13] and use as fiber[12] and planar waveguide polarizers[14] have been investigated. Given the unique 2D structure of graphene, its optical properties can be more fully utilized when surface waves propagate through the graphene plane. Under total internal reflection (TIR), a fraction of the incident energy

can penetrate through the interface of medium 1 and medium 2; this energy fraction propagates along this interface and is known as the evanescent field. At $z=0$, the intensity components (I_{0x}, I_{0y} and I_{0z}) of the evanescent fields induced by TE (s-polarized) and TM (p-polarized) incident light are shown in Fig. 1b[18] with $n_1=1.61$ and $n_2=1.41$. The intensities of the evanescent field for the s- and p-polarized incident lights at $z=0$ are $I_{0s}=I_{0y}$ and $I_{0p}=I_{0x}+I_{0z}$. When graphene is placed between two media, the relative proportions of the intensity components that are parallel or orthogonal to the graphene plane will result in different propagation behaviors for s- and p-polarized light. Furthermore, the x, y, and z intensity components are also dependent on the change of n_2 when n_1 is fixed (Fig. 1c). Thus, it is expected that the reflectance of the structure shown in Fig. 1a will differ significantly for distinct proportions of incident s- and p-polarized light.

Using a derivative total reflection method (Fig. S3), the reflectance of the prism/graphene/substrate tri-layer structure can be obtained for s- and p-polarized incident light (Fig. 1d). The refractive indexes of the substrate can be changed by employing different solvents, such as water (1.33174), alcohol (1.36169), butyl alcohol (1.39466), N,N-dimethylformamide (1.47497), dimethylamine (1.43697), and chloroform (1.44176). Fig. 1D presents the experimental results of the reflectance for s- and p-polarized light with different values of $\Delta n = n_1 - n_2$ using a derivative total reflection method (See Method and Fig. S3). Four-layer graphene grown by chemical vapor deposition (CVD) was transferred to the bottom of a prism. There are many kinds of methods to define the number of graphene layers, such as the transmittance, Raman spectroscopy[19] and SPR[20]. In our experiment, the number of graphene layers was defined by the transmittance (Fig. S4) and Raman spectroscopy (Fig. S5). The absorbance of graphene samples with different number of layers were shown in Fig. S4. When the absorbance of graphene sample is about 9%, the number of graphene layers is determined to be four by combining with it Raman spectroscopy as shown in Fig. S5. And the optimized

number of graphene layer for this sensor application is four in our current studies. The changes in n_2 were achieved using different liquid solvents. The reflectance R of the tri-layer structure for s-polarized light is much smaller than the reflectance for p-polarized light, which indicates that graphene has a greater absorption for s-polarized light when transmission is prevented by TIR[21].

The general theory regarding light diffraction by tri-layer structures (Fig. 1a) that consist of a loss layer (graphene) sandwiched between two semi-infinite dielectrics (medium 1 and medium 2) states that the manner in which the transition takes place is also governed by Maxwell's boundary conditions, which state that the tangential components of the electric (**E**) and magnetic (**H**) fields are continuous across boundaries[22]. The intermediate graphene layer has a complex optical constant with $\hat{n}=n+ik$, where n is the real refractive index of graphene and k is its extinction coefficient[23–25]. The thickness d is relative to the number of layers of graphene (e.g., $d=0.34$ nm for a single layer of graphene). Based on the boundary conditions and Snell's law, the reflectance of tri-layer structures can be obtained for s- and p-polarized light (see Supplementary theory). As shown in Fig. S2, the graphene layer stores more energy for TE waves than for TM waves. Thus, in situations involving the total reflectance of light, the reflectance of TE waves is less than that of TM waves. The reflectances of s- and p-polarized light appear to vary with the incident angle of the light and the refractive indexes of the substrates. Thus, the reflectance differences observed in this experiment are a function of both the incident angle and the refractive indexes of the media that are used. The polarization-dependent reflection experiments of single-layer and bi-layer graphene were performed. The corresponding results were shown in Fig. S6. The theoretical simulations based on Maxwell's boundary condition are in agreement with the experimental results, which supports our theoretical model.

For a given incident angle (e.g., 75°), the difference ($\Delta R = R_{\text{TM}} - R_{\text{TE}}$) in reflectance between s- and p-polarized incident light is strongly dependent on Δn (Fig. 1f). Figures 1e and 1f (solid line) provide the theoretical results generated by Maxwell's boundary conditions (see Supplementary theory) with $\hat{n}=2.6+1.6i$ and $d=1.36$ nm (four layers). The observed value of $k=1.6$ is slightly larger than the reported value of $k=1.3$[25]. One possible reason for this discrepancy is that the graphene sample used in this analysis was grown using CVD and therefore has a less even distribution than the mechanically exfoliated graphene. When medium 1 and the graphene layer are fixed, the change in the refractive index of medium 2 can be determined by measuring ΔR for a given incident angle.

Device design. We designed a simple, real-time refractive index measuring system that used GRIS in combination with a microfluidic system. The experimental setup is shown in Fig. 2a and uses a 523 nm continuous wave laser as a light source. First, circularly polarized light obtained by adjusting a Glan-Taylor polarizer and a quarter-wave plate was focused on the GRIS at the center of its microfluid channel. The inset of Fig. 2a shows the structure of the GRIS, and the full diagram of the microfluid GRIS is provided in Fig. S8. Second, a multi-layer graphene coating was transferred to a right-angle prism using CVD and the cast microfluid channel was bonded to the graphene layer to form a microfluid channel/graphene/prism sandwich structure (see Fig. S7 for the detailed process). In this step, the focused spot must be small enough to ensure that it can be fully irradiated inside the microfluid channel. Third, the incident angle of circularly polarized light was adjusted in accordance with the refractive index of the fluid to be measured, allowing TIR to occur as incident light passed through the microfluid channel. Fourth, the reflected light was separated into s- and p-polarized light using a polarization beam splitter (PBS) and then detected by a balanced
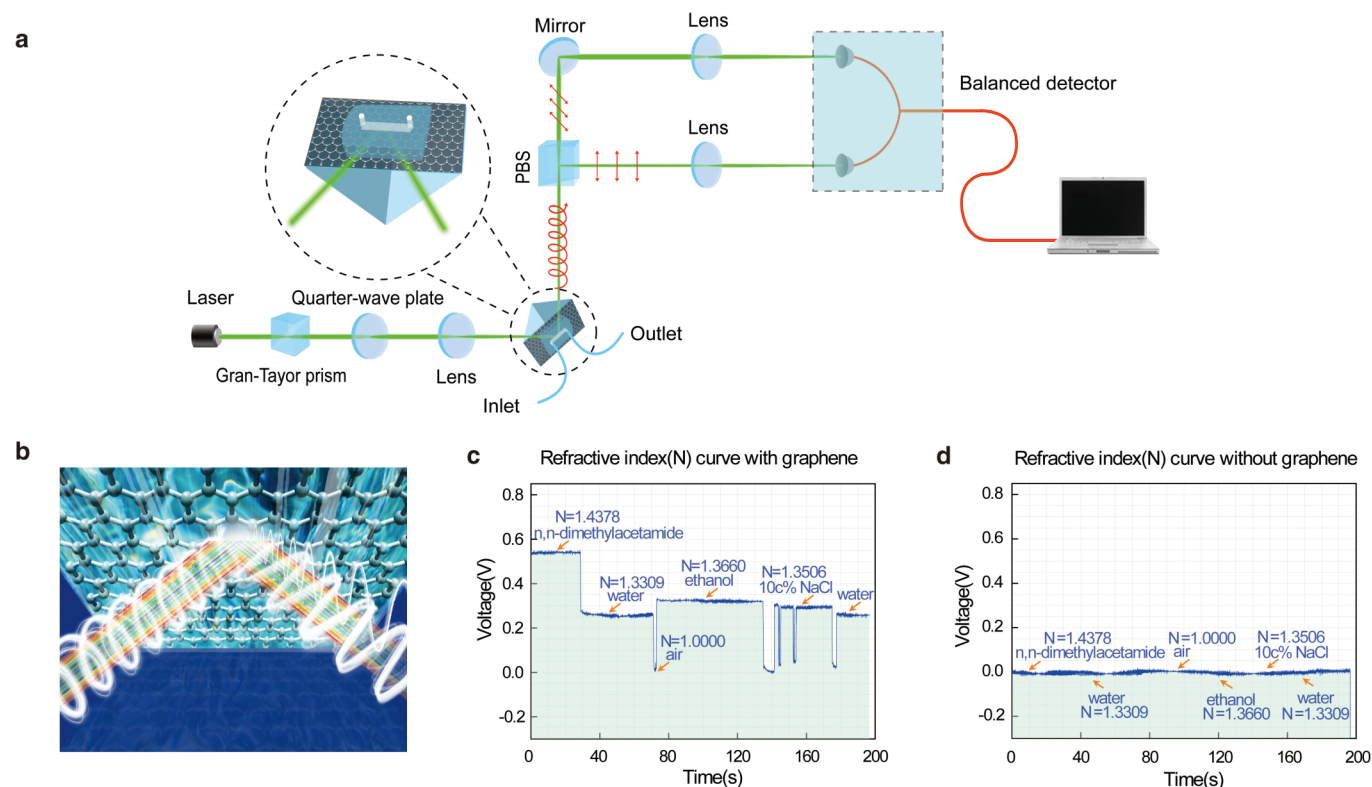
Figure 2 | A sensitive, real-time microfluid refractive index measuring system. (a) A schematic illustration of the measuring system. The enlarged diagram shows the sandwiched structure of the GRIS. PBS separated the circularly polarized light into s- and p-polarized lights. (b) A schematic illustration of the GRIS. The light source can be a laser of any wavelength or even natural light. The absorption of s-polarized light is much greater than that of p-polarized light when fluid is flowing. (c and d) The real-time voltage signal change of microfluid with and without graphene when injecting N,N-dimethyl acetamide, deionized water, air, ethanol, air, a solution of 10% NaCl, air and water successively at a flow rate of 10 μL/s.

detector. A balanced detector consisted of two well-matched photodetectors was used to detect the difference between the photocurrents in the two optical input signals[26]. Due to the polarization-sensitive absorption of graphene under total internal reflection, the intensity of the p-polarized light changed little before and after microfluid injections, whereas the microfluid injection greatly altered the measured intensity of the s-polarized light, as shown in Fig. 2b and Fig. 1d. The signal from the balanced detector is measured relative to the difference $\Delta R = R_{TM} - R_{TE}$ in reflectance between the s- and p-polarized incident lights. Thus, the signal from the balanced detector can be used to monitor the change in the refractive index of the fluid. After a calibration using standard liquids known, the GRIS can be used for refractive index measuring. Furthermore, before signal measurements, a substance (generally air or water) should be chosen to calibrate the detector, and the output voltage of the balanced detector should be adjusted to 0 V for this reference substance. During the measurement process, the refractive index of the internal microfluid channel at each moment corresponds to a particular voltage calculated by subtracting the intensity of the s-polarized light from that of the p-polarized light measured by the balanced detector. The voltage varies with the microfluid's refractive index; fluids with larger refractive indexes produce higher calculated voltages.

Discussion

One of the prominent features of the GRIS is its broad measuring range, as its signal depends on the value of Δn. To demonstrate this advantage, an experiment was conducted at room temperature with an incident angle of 83°; under these conditions, the refractive index of the prism was 1.51. When the incident power before the GRIS was 0.202 mW, the power of the p-polarization in front of the balanced detector was 10.33 µW. Subsequently, using air for calibration purposes, we injected N,N-dimethyl acetamide, deionized water, air, absolute ethyl alcohol, air, a solution of 10% NaCl, air and water in turn at a flowing speed of 10 µL/s, generating a relationship curve indicating the real-time voltage signal change of the microfluid, as shown in Fig. 2c. The real-time refractive index range was easily measured for refractive indexes ranging from 1 to 1.438. In fact, the dynamic range of the GRIS depends on the refractive index of the prism. If a prism with a refractive index of 1.71 is used, the refractive index of chlorobenzene (1.57) can be easily measured. The most commonly used method of measuring real-time refractive indexes employs an SPR sensor based on the modulation of incident angles. The dynamic range of SPR can readily be extended to be lower or higher, using different prism materials having various dielectric constants[27]. However, the change of prism materials is not convenient in real-time monitoring. The dynamic range of SPR may be restricted, when a fixed prism is used in refractive index measurements[28]. Therefore, the GRIS provides a reliable platform for measuring the refractive index of more complicated micro-fluids with a larger dynamic refractive index range. Figure 2d illustrates the results for tests in which the PDMS micro-fluid channel was directly bonded to the prism without a graphene sensor layer between them. Under the same conditions detailed above for the GRIS, this control was successively placed in the aforementioned fluids, producing a voltage signal that was always close to 0 V for each different liquid input. The lack of a distinctive pattern of alteration between the liquids demonstrates that the novel properties of graphene play a key role in the GRIS's detection ability.

As a sensing layer, graphene offers good, stable real-time performance. Fig. 2c shows that the voltage signal changes quite predictably and rapidly upon the inflow of each different fluid into the microfluid channel. During the injection of the 10% NaCl solution, the voltage signal exhibited a transitory decrease caused by air bubbles in the solution[29]. Nevertheless, the evident advantages of using graphene as a sensing layer are manifold. First, with its perfect 2d

structure, graphene possesses desirable mechanical properties and chemical stability, which means that a graphene sensing layer is difficult to damage. Second, the nanometer-order thickness of graphene greatly increases the propagation distance of evanescent waves in liquid, thereby producing a more accurate detection result. The velocity distribution of the fluid in a micro-fluid channel is known to be uneven because the fluid flows more slowly as it approaches the sensing layer; thus, if the propagation distance (in the z direction) of the evanescent waves in the fluid is short, the detected result would be subject to larger time-delay errors, resulting in poor real-time performance. For these reasons, graphene sensors provide longer service life, better real-time performance and greater versatility in fluid measurements.

The rapid response of the GRIS makes it possible to measure a fluid using a faster flow rate and to quickly reflect the changes in refractive indexes during a process of rapid fluid flow. In the experiment, we simultaneously detect the two values by using a balanced detector. The GRIS's response speed is dependent on the response time of the detector and data acquisition equipment. To illustrate more accurate measurement using high collecting frequency, we combined rapid peristalsis (300 µL/s) and data collection (100 kHz). The data were initially collected at a frequency of 10 kHz with an interval of 100 µs. As shown in Fig. 3a, during successive injections of air and deionized water at different flow rates, the voltage changed by nearly 10 V is both nearly identical for different fluids and quite reproducible for different flow rates. At different flow rates, the voltage changed continuously at lower speeds and quite discontinuously at higher speeds. In particular, speeds approaching 300 µL/s led to a large voltage interval. These changes indicate that the refractive index change of micro-fluids at higher speeds cannot be measured with good integrity at the collecting frequency of 10 kHz, which made it difficult for the sensor to conduct real-time measurements at high speeds. For this reason, we changed the frequency of data collection to 100 kHz with an interval of 10 µs and repeated the above experiments under the same conditions. The experimental data generated after this modification indicated that minor changes in the refractive index were clearly evident at both a low speed of 5 µL/s and a higher speed of 300 µL/s (Fig. 3b). To better demonstrate the significance of a higher response speed in real-time refractive index measurements, we compared the curves obtained at the two different collecting frequencies at the speed of 300 µL/s (Fig. 3c). The comparison shows that the two curves are almost identical; thus, this experiment exhibits high stability. Most importantly, the refractive index change at an interval of 10 µs can be better measured at the collecting frequency of 100 kHz, which produces a continuous curve. In contrast, the data points measured at a frequency of 10 kHz are rather discontinuous and can only indicate rough trends. Therefore, a higher response speed facilitates the more accurate measurement of tiny changes in the refractive index; this property is particularly important for measuring refractive indexes during rapid-response processes, which are common in many biological and chemical interactions. In fact, the GRIS's response speed is theoretically dependent on the response time of the balanced detector and data acquisition equipment; the equipment used in this experiment can reach 10 ns and 340 kHz. However, the response speed of a traditional refractive index sensor, including SPR refractive index sensors, is generally on the order of milliseconds.

Moreover, the GRIS has high resolution and sensitivity. To experimentally demonstrate this property, we generated a curve (see Fig. 4a) representing the voltage changes associated with injecting deionized water, a solution of 0.1% NaCl and a solution of 20% NaCl successively in the microfluid channel by shining a 13.03 mW light at the GRIS. Under the same conditions, the refractive indexes of deionized water and 0.1% NaCl solution were determined to be 1.33091 and 1.33139, respectively (see Table S1), which differ by 0.00048. The inset of Fig. 4A shows that the corresponding voltage difference
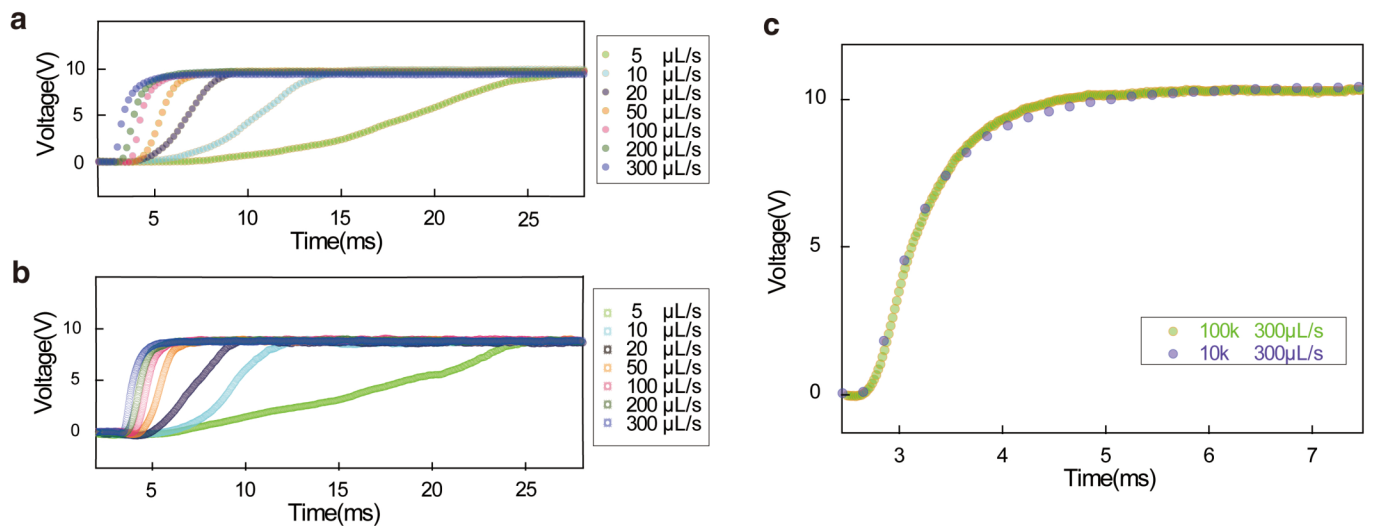
Figure 3 | An evaluation of the response speed performance of the GRIS. (a and b) The real-time voltage curve at collection frequencies of 10 kHz and 100 kHz obtained by successively injecting air and deionized water at different flow rates. The flow rate ranges from 5 μL/s to 300 μL/s. (c) The purple dots represent the real-time voltage curve at a collection frequency of 10 kHz and a flow rate of 300 μL/s. The light-green dots represent the real-time voltage curve at a collection frequency of 100 kHz and a flow rate of 300 μL/s.

between the deionized water and the 0.1% NaCl solution is ~245 mV and the size of the voice signal is ~45 mV. Hence, the resolution which can be measured in the experiment is 1×10^{-4}. We defined sensitivity for the refractive index to be a slope of the straight line, dv/dn, where v is the voltage signal and n is the refractive index. Because the relationship between the change in the refractive index and the change in voltage is considered to be roughly linear within a

small range, the dv/dn obtained by the experiment was 5.1×10^5 mV/UIR. This result is comparable to the sensitivity of an SPR refractive index sensor $(10^4–10^6/UIR)$[30,31].

In fact, both the resolution and sensitivity of the GRIS are strongly correlated with the power of the incident light (Fig. 4b), and both of them can be further improved. On one hand, under a given incident power, the voltage signal in measurements is higher for thicker NaCl
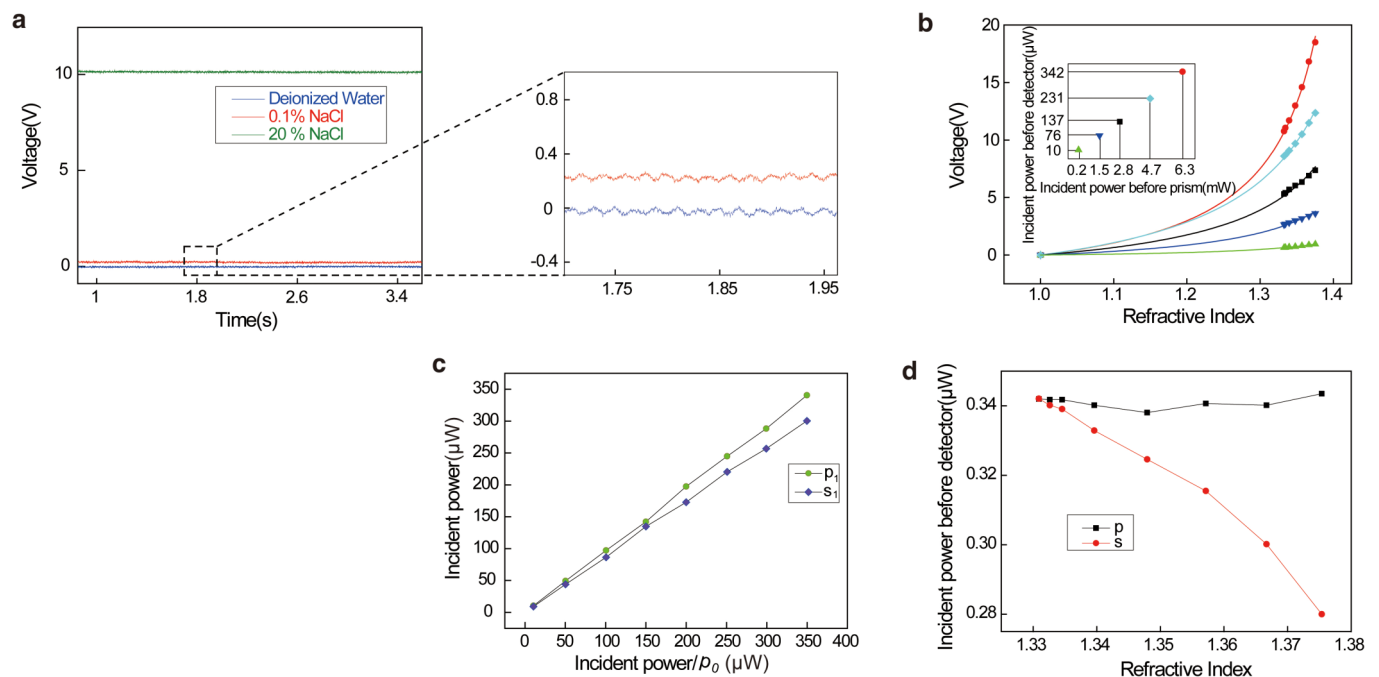
Figure 4 | The resolution performance and incident power dependence of the GRIS. (a) A curve representing the change in voltage after injecting deionized water, a solution of 0.1% NaCl and a solution of 20% NaCl into the micro-fluid channel, respectively. The incident light power is 13.03 mW before the prism. The inset shows that the corresponding voltage difference between deionized water and a solution of 0.1% NaCl is 245 mV and the size of voice signal is ~45 mV. (b) The incident power before the prism is, from bottom to top, 0.2, 1.5, 2.8, 4.7, and 6.3 mW. The inset indicates the correspondence between the incident power before the prism and incident power before the detector. Each point corresponds to a different concentration of the sodium chloride solution: from left to right, 1, 2, 5, 10, 15, 20, and 25%. (c) Using the p-polarized light power P_0 of deionized water as calibration, a solution of 20% NaCl was injected into the GRIS to determine the changes in polarization status S_1 and P_1 for this solution under different incident powers P_0. (d) The power of s- and p-polarized light before the detector after injecting NaCl solutions with different concentrations into the microfluid channel.

solutions, which has a higher refractive index. How the voltage changes with the refractive index of substrates can be theoretically (solid lines in Fig. 4b) modeled well based on the boundary conditions and Snell's law (see Supplementary theory). Over a large range, the change in the refractive index with voltage is nonlinear. if the refractive index of the liquid is close to the that of prism, the voltage signal from measurements is increased and the sensitivity should increase too. On the other hand, as shown in Fig. 4b, if we use this method to measurement the refractive index of two solutions with different refractive index at identical incident power, the voltage signal is different for them and the signal difference increase with the incident power used.

Thus, enhancing the incident power could be a way of improving resolution and sensitivity of the GRIS (as the red line and green line), but the incident power should be lower than the damage thresholds of the graphene and the detector. The maximum incident power adopted in our experiment is 13.03 mW, which is much lower than the damage threshold ($>$W) of graphene.

To verify the influence of incident powers on the sensitivity, we measured the incident power before detector at different incident power for s- and p- polarized light. In our measurements, we used deionized water to calibrate the GRIS, then a 20% NaCl solution was injected into the GRIS and the intensity change (see Fig. 4c) of s- and p- polarized light under different incident powers applied to the detector was measured. Then, we changed the incident power and repeat the calibration and measurements. The results are shown in Fig. 4c. In the figure, P_0 represents the calibrated power of deionized water and P_1 and S_1 are defined as the powers of the p- and s-polarization, respectively, upon the injection of a solution of 20% NaCl. As shown in Fig. 4c, the injection of a 20% NaCl solution only slightly changes the p-polarization power relative to the p-polarization power calibrated using deionized water. The larger the calibrated power (50, 100, 150, 200, 250, 300, and 350 mW), the larger the difference is between the powers of s- and p-polarization. Figure 4d illustrates the changes in the status of s-polarization and p- polarization that are obtained by injecting NaCl solutions of different concentrations into the microfluidic channel when the incident power is fixed at 6.73 mW and deionized water is used to calibrate the GRIS. As shown in Fig. 4d, the p-polarized light intensity changes only slightly (remaining at approximately 0.34 mW) when NaCl solutions with different concentrations was injected, whereas the s-polarized light intensity changes from 0.34 mW to 0.28 mW, which is consistent with the relationship observed between changes in the refractive index and changes in the measured voltage values (Fig. 4b).

To evaluate the potential of the GRIS under real conditions, real-time monitoring of the concentrations of glucose and NaCl solutions was attempted and the performance of the sensor was analyzed. In production processes, it is often necessary to conduct real-time measurements of the concentration of a liquid, such as a solution of glucose or NaCl. In this study, we illustrate the real-time measurement curves for a NaCl solution and a glucose solution in Fig. 5a and Fig. 5b, respectively. In these curves, the incident power is 6.73 mW, the reference power is that of the p-polarization, 342 µW, and air is used to calibrate the GRIS. NaCl or glucose solutions of different concentrations are injected into the channel, proceeding from lower to higher densities. The figure clearly shows that the voltage values of NaCl and glucose solutions of different concentrations at any time correspond to the refractive index (see Tabs. S1 and S2); thus, this sensor can achieve a high response within a broad range and is able to measure the change in the refractive index of a liquid in a simple fashion.

We have demonstrated that graphene sandwiched between two dielectric layers has a stronger absorption for s-polarized light than for p-polarized light under TIR. These different absorption behaviors for s- and p-polarized light make graphene suitable for use as an optical detector of refractive indexes. The sensitive and real-time

monitoring of the refractive index was shown using a graphene-based optical sensor that has a broad dynamic refractive index range from 1.0 to 1.438, a fast response time of $\sim$10 µs, a high sensitivity of 10^5 RIU^{-1}, and excellent stability; these qualities are all essential for a versatile refractive index sensor. The flexibility and ease of functionalization of graphene sheets could also enable radically different refractive index sensors to be designed. For example, graphene could be integrated with flexible substrates and plastic materials. Alternatively, it could be used in novel geometries, e.g., as a flexible sensor. The recent development of large-scale graphene synthesis and transfer techniques[32], as well as the structural modification of graphene by chemical or biological molecules, ensures that graphene will become the basis for powerful label-free monitoring methods for chemical or biomolecular interactions.

Methods

Preparation for graphene/prism structure. As a mature method of producing graphene devices, the transfer method of using thermal release tape can instantly etch Ni layers and easily produce large scale graphene devices. The polymer supports thermal release tape (TRT) was attached to the CVD-made, Ni-based graphene to form a structure of TRT/graphene (G)/Ni/SiO$_2$/Si. The multilayer structure was then soaked in deionized water. For ultrasonic processing in a few minutes, the TRT/G/Ni layers are detached from SiO$_2$. Then, putting the TRT/G/Ni layers into an aqueous iron (III) chloride (FeCl$_3$) solution (1 M) to remove the nickel layers. After that, process the prism surface with plasma oxygen cleaning for a few minutes, and then cover the TRT/G layers on the prism surface and press them tightly to some extent.
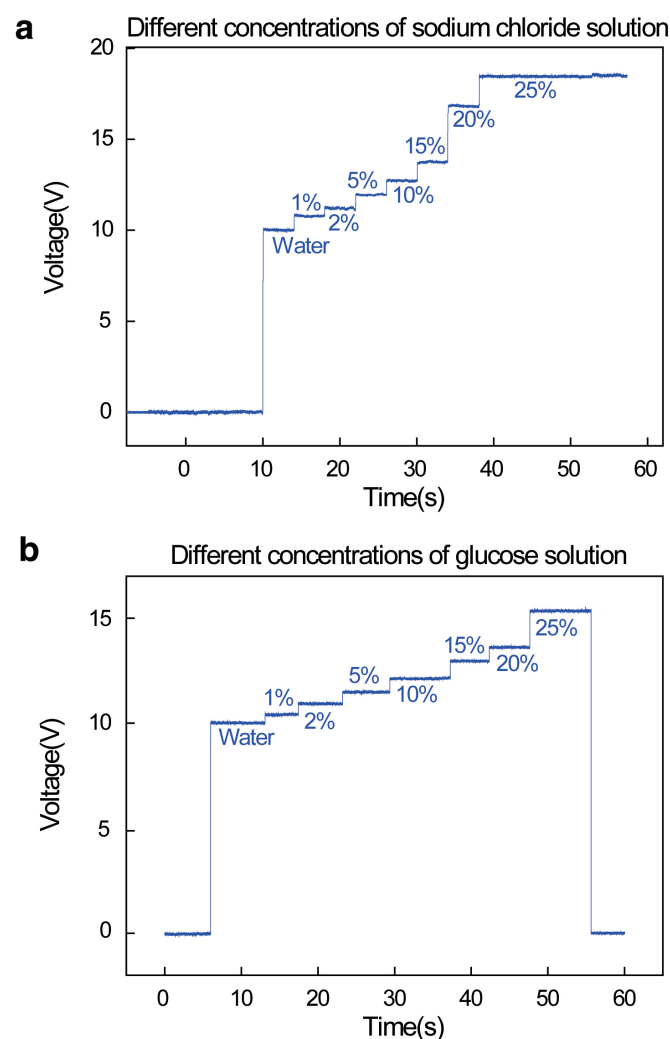
Figure 5 | The real-time measured voltage curves. (a) Different concentrations of sodium chloride solutions. (b) Different concentrations of glucose solutions.

Then, put the TRT/G/Prism layers into a vacuum drying oven for heating till 100°C, so as to detach graphene layers with TRT completely. At last, putting the G/Prism layers into a acetone solution to wash off the residual glue, and then store it in the vacuum line of the fume hood. Raman spectroscopy was carried out using RENISHAW RM2000 Raman system equipped with a 514 nm laser source and 50× objective lens (Fig. S5).

A derivative total reflection method. Light at wavelength of 632.8 nm from a He-Ne laser is split into incident and reference beams by a beam splitter M. After passing through a half-wave plate H and a polarizer P, the incident beam reached an equilateral prism fixed on a rotation stage (M-038, PI). PD1 and PD2 are the two detectors of a Dual-channel power meter (PM320E, Thorlabs). PD1 is used for monitoring the instantaneous fluctuations of the laser energy. PD2 is used to measure the final light reflected by the prism. D is an aperture diaphragm to block the scattering light. The experiment setup was first calibrated by deionized water. Reflectance curves as a function of incident angle were recorded. At 632.8 nm, the refractive index of prism is 1.61656. The refractive index of substrate can be changed by using different solvents of water (1.33174), alcohol (1.36169), butyl alcohol (1.39466), N,N-Dimethylformamide (1.47497), dimethylamine (1.43697), chloroform (1.44176).

Preparation for microfluid channel. Poly(dimethylsiloxane) (PDMS) has been shown to be biocompatible and it is also chemically stable. So it is noble material for fabrication of microfluid channel. Use computer-aided design (CAD) software programs to design a pattern. The photoresist mask was etched with electron beam lithography. Spin coat negative photoresist (SU-8) to the Si base at a speed of 1,100 r/min in 50 s and then dry it at 110°C. Then, cover the photoresist mask on the negative photoresist (SU-8)/Si layers and expose them to ultraviolet light and then photographic develops to get the master. Use a balance to weigh 70 g of Sylgard 184 silicone elastomer base and 7 g of Sylgard 184 elastomer curing agentfully (10:1 ratio) and mix them fully. Then, lay the liquid mixture into vacuum line of the fume hood to trapped bubbles for one hour. After that, pour the liquid mixture on the master, place the dish containing both the master and PDMS prepolymer in an oven set to 70°C and cure it for 3 h. Then , with a plier peel the solidified PDMS microfluid channel off the master.

Preparation for GRIS with microfluid chanel. Process the prior prepared G/Prism structure and PDMS microfluid channel in a plasma oxygen cleaning with 150 W in power for 30 s, then, irreversibly adhered G/Prism structure with PDMS microfluid channel to get the GRIS with microfluid chanel.

1. Geim, A. K. Graphene: Status and Prospects. *Science* **324**, 1530–1534 (2009).
2. Schedin, F., Geim, A. K., Morozov, S. V., Hill, E. W., Blake, P. *et al.* Detection of Individual Gas Molecules Adsorbed on Graphene. *Nat. Mater.* **6**, 652–655 (2007).
3. Chen, C. W., Hung, S. C., Yang, M. D., Yeh, C. W., Wu, C. H. *et al.* Oxygen sensors made by monolayer graphene under room temperature. *Appl. Phys. Lett.* **99**, 243502 (2011).
4. He, R. X., Lin, P., Liu, Z. K., Zhu, H. W., Zhao, X. Z. *et al.* Solution-Gated Graphene Field Effect Transistors Integrated in Microfluidic Systems and Used for Flow Velocity Detection. *Nano Lett.* **12**, 1404–1409 (2012).
5. Newaz, A. K. M., Markov, D. A., Prasai, D. & Bolotin, K. I. Graphene Transistor as a Probe for Streaming Potential. *Nano Lett* **12**, 2931–2935 (2012).
6. Shao, Y., Wang, J., Wu, H., Liu, J., Aksay, Ilhan A. & Lin, Y. Graphene Based Electrochemical Sensors and Biosensors: A Review. *Electroanalysis* **22**, 1027–1036 (2010).
7. Liu, Y., Dong, X. & Chen, P. Biological and chemical sensors based on graphene materials. *Chem. Soc. Rev.* **41**, 2283–2307 (2012).
8. Stine, R., Robinson, J. T., Sheehan, P. E. & Tamanaha, C. R. Real-Time DNA Detection Using Reduced Graphene Oxide Field Effect Transistors. *Adv. Mater.* **22**, 5297–5300 (2010).
9. Bonaccorso, F., Sun, Z., Hasan, T. & Ferrari, A. C. Graphene photonics and optoelectronics. *Nat. Photonics* **4**, 611–622 (2010).
10. Bao, Q. & Loh, K. P. Graphene Photonics, Plasmonics, and Broadband Optoelectronic Devices. *ACS Nano* **6**, 3677–3694 (2012).
11. Mikhailov, S. A. & Ziegler, K. New electromagnetic mode in graphene. *Phys. Rev. Lett.* **99**, 016803 (2007).
12. Bao, Q., Zhang, H., Wang, B., Ni Candy, Z., Lim, H. Y. X. *et al.* Broadband graphene polarizer. *Nat. Photonics* **5**, 411–415 (2011).
13. Vakil, A. & Engheta, N. Transformation Optics Using Graphene. *Science* **332**, 1291–1294 (2011).
14. Kim, J. T. & Choi, S. Y. Graphene-based plasmonic waveguides for photonic integrated circuits. *Opt. Express* **19**, 24557–24562 (2011).
15. Stanley, G. F. *Refractometers: Basic Principles* (Bellingham & Stanley Ltd. 1989).
16. Homola, J. *Surface Plasmon Resonance Based Sensors* (Springer Berlin Heidelberg, 2006).
17. Nair, R. R., Blake, P., Grigorenko, A. N., Novoselov, K. S., Booth, T. J. *et al.* Fine structure constant defines visual transparency of graphene. *Science* **320**, 1308–1308 (2008).
18. Axelrod, D., Burghardt, T. P. & Thompson, N. L. Total internal reflection fluorescence. *Annu. Rev. biophys. Bioeng.* **13**, 247–268 (1984).
19. Graf, D., Molitor, F., Ensslin, K., Stampfer, C., Jungen, A., Hierold, C. & Wirtz, L. Spatially Resolved Raman Spectroscopy of Single- and Few-layer Graphene. *Nano Lett.* **7**, 238–242 (2007).
20. Sosan Cheon, Kenneth David Kihm, Jae Sung Park, Joon Sik Lee, Byeong Jun Lee, Hyeoungkeun Kim & Byung Hee Hong. How to optically count graphene layers. *Opt. Lett.* **37**, 3765–3767 (2012).
21. Thongrattanasiri, S., Koppens, F. H. L. & Javier Garcia de Abajo, F. Complete Optical Absorption in Periodically Patterned Graphene. *Phys. Rev. Lett.* **108**, 047401 (2012).
22. Born, M. & Wolf, E. *Principles of optics.* (Cambridge University Press, 1999).
23. Bruna, M. & Borini, S. Optical constants of graphene layers in the visible range. *Appl. Phys. Lett.* **94**, 031901 (2009).
24. Weber, J. W., Calado, V. E. & van de Sanden, M. C. M. Optical constants of graphene measured by spectroscopic ellipsometry. *Appl. Phys. Lett.* **97**, 091904 (2010).
25. Blake, P., Hill, E. W., Castro Neto, A. H., Novoselov, K. S., Jiang, D. *et al.* Making graphene visible. *Appl. Phys. Lett.* **91**, 063124 (2007).
26. Philipp Kukura, Michele Celebrano, Alois Renn & Vahid Sandoghdar. Single-Molecule Sensitivity in Optical Absorption at Room Temperature. *J. Phys. Chem. Lett.* **1**(23), 3323–3327 (2010).
27. Kenneth D. Kihm. Surface plasmon resonance reflectance imaging technique for near-field (~100 nm) fluidic characterization. *Experiments in Fluids* **48**(4), 547–564 (2010).
28. Antonino Parisi, Alfonso C. Cino, Alessandro C. Busacca, Matteo, Cherchi & Stefano Riva-Sanseverino. Integrated Optic Surface Plasmon Resonance Measurements in a Borosilicate Glass Substrate. *Sensors* **8**, 7113–7124 (2008).
29. Ledesma-Aguilar, R., Nistal, R., Hernández-Machado, A. & Pagonabarraga, I. Controlled drop emission by wetting properties in driven liquid filaments. *Nat. Mater.* **10**, 367–371 (2011).
30. Ludovic, S. Live, Jean-Francois Masson, High Sensitivity of Plasmonic Microstructures near the Transition from Short-Range to Propagating Surface Plasmon. *J. Phys. Chem. C* **113**, 10052–10060 (2009).
31. Im, H., Sutherland, J. N., Maynard, J. A. & Oh, S. H. Nanohole-Based Surface Plasmon Resonance Instruments with Improved Spectral Resolution Quantify a Broad Range of Antibody-Ligand Binding Kinetics. *Anal. Chem.* **84**, 1941–1947 (2012).
32. Kim, K. S. *et al.* Large-Scale Pattern Growth of Graphene Films for Stretchable Transparent Electrodes. *Nature* **457**, 706 (2009).

Author contributions
The experiments were conceived, designed and carried out by X.F., Z.B.L. and Z.C.D., X.D.C. and X.Q.Y. performed graphene and transfer. X.T.K. and Z.B.L. contributed to the interpretation of the data and developed analytical and computational theoretical tools. J.G.T., Q.Y., C.P.Z. and Y.S.C. analysed and interpreted the data. Z.B.L., X.F. and J.G.T. wrote the manuscript with the assistance of all other co-authors.

Additional information
Supplementary information accompanies this paper at http://www.nature.com/scientificreports

Competing financial interests: The authors declare no competing financial interests.

How to cite this article: Xing, F. *et al.* Sensitive Real-Time Monitoring of Refractive Indexes Using a Novel Graphene-Based Optical Sensor. *Sci. Rep.* **2**, 908; DOI:10.1038/srep00908 (2012).